Proc. Indian Acad. Sci. (*Chem. Sci.*), Vol. 113, No. 4, August 2001, pp 257–273

Spectral, magnetic and biological studies of 1,4-dibenzoyl-3-thiosemicarbazide complexes with some first row transition metal ions

NAND K SINGH*,[1], SATY B SINGH [1], ANURAAG SHRIVASTAV [1] and SUKH M SINGH [2]
[1]Department of Chemistry, and [2]School of Biotechnology, Banaras Hindu University, Varanasi 221 005, India
e-mail: nksingh@banaras.ernet.in

MS received 29 January 2001; revised 30 March 2001

Abstract. The ligand 1,4-dibenzoyl-3-thiosemicarbazide (DBtsc) forms complexes [M(DBtsc-H)(SCN)] [M = Mn(II), Co(II) or Zn(II)], [M(DBtsc-H)(SCN)(H_2O)] [M = Ni(II) or Cu(II)], [M(DBtsc-H)Cl] [M = Co(II), Ni(II), Cu(II) or Zn(II)] and [Mn(DBtsc)Cl_2], which have been characterized by elemental analyses, magnetic susceptibility measurements, UV/Vis, IR, ^{1}H and ^{13}C NMR and FAB mass spectral data. Room temperature ESR spectra of the Mn(II) and Cu(II) complexes yield <*g*> values, characteristic of tetrahedral and square planar complexes respectively. DBtsc and its soluble complexes have been screened against several bacteria, fungi and tumour cell lines.

Keywords. 3*d*-Metal complexes; thiosemicarbazide; antitumour activity.

1. Introduction

Thiosemicarbazides and their complexes have been found to possess a wide variety of biological activities against bacteria [1], fungi [2] and certain type of tumours [3]. Some work has been done on the transition metal complexes of substituted thiosemicarbazides particularly the 1-aroyl-4-aryl derivatives [4–8]. 1,4-Dibenzoyl-3-thiosemicarbazide contains oxygen, sulphur and nitrogen as potential donor atoms and is liable to form deprotonated complexes by loss of hydrazinic proton(s) via enolisation/thioenolisation. In view of the absence of previous work on 1,4-diaroylthiosemicarbazides, we have prepared the complexes of 1,4-dibenzoyl-3-thiosemicarbazide (figure 1) with 3*d*-metal ions and studied their antifungal, antibacterial and *in vitro* antitumour activity.

2. Experimental

2.1 *Starting material*

All chemicals used were of analytical reagent or equivalent grade. Benzoyl isothiocyanate [9], benzoyl hydrazine [10] and metal thiocyanates were prepared by literature methods.

*For correspondence

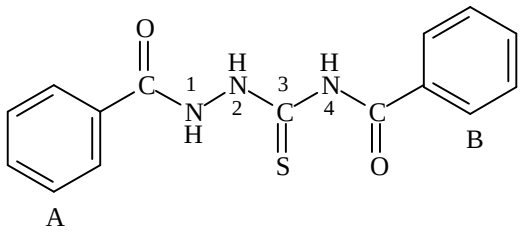

Figure 1. Structure of the ligand 1,4-dibenzoyl-3-thiosemicarbazide (DBtsc).

2.2 *1,4-Dibenzoyl-3-thiosemicarbazide (DBtsc)*

1,4-Dibenzoyl-3-thiosemicarbazide (DBtsc) [11] was prepared by refluxing a suspension of benzoyl hydrazine (1·36 g, 10 mmol) in dry benzene (20 cm^3) with an equimolar amount of benzoyl isothiocyanate (1·97 g, 10 mmol) for 4 h. On cooling, the solid that separated was filtered, washed with benzene (to remove excess of benzoyl isothiocyanate) and water, dried and recrystallized from hot EtOH, m.p. 172°C (Lit. 172°C).

2.3 *Preparation of the complexes*

[M(DBtsc-H)(SCN)] (M = Co(II) or Zn(II)), [Ni(DBtsc-H)(SCN)(H_2O)], [M(DBtsc-H)Cl] (M = Cu(II), Ni(II) or Zn(II)) and [Mn(DBtsc)Cl_2] were prepared by refluxing the ethanolic solutions (20 cm^3) of the respective metal (II) thiocyanate/chloride (3 mmol) and the ligand (0·9 g, 3 mmol) for ≈1 h. The complexes which precipitated on cooling were filtered, washed with cold EtOH and dried *in vacuo*. The [Mn(DBtsc-H)(SCN)] and [Co(DBtsc-H)Cl] complexes were isolated by mixing and stirring the ethanolic solutions (20 cm^3) of the respective metal (II) thiocyanate/chloride (3 mmol) and the ligand (0·9 g, 3 mmol), while [Cu(DBtsc-H)(SCN)(H_2O)] was isolated by stirring together the DMF (20 cm^3) solutions of $Cu(SCN)_2$ (3 mmol) and the ligand (0·9 g, 3 mmol), for 10–15 h. The precipitated complexes were filtered, washed with the respective solvent and dried *in vacuo*.

3. Physical measurements

The complexes were analysed for their metal contents, following standard procedures [12] after decomposition with a mixture of conc. HNO_3 and HCl, followed by conc. H_2SO_4. Sulphur and chloride were determined as $BaSO_4$ and AgCl, respectively. Carbon, hydrogen and nitrogen were estimated on a Perkin–Elmer 240C model microanalyser. Magnetic susceptibility measurements were made at room temperature on a Cahn–Faraday balance using Hg[$Co(NCS)_4$] as calibrant. Electronic spectra were recorded on a Cary-2390 UV-Visible spectrophotometer in DMF solution. IR spectra were recorded in the 4000–400 cm^{-1} region as Nujol mulls on a Jasco FT/IR-5300 spectrophotometer. ^{1}H- and ^{13}C-NMR spectra were recorded in DMSO-d_6 on a Jeol F*x*-90QFT NMR spectrometer using TMS as internal reference. ESR spectra were recorded on an X-band spectrometer model EPR-112 using DPPH as a <*g*> marker. Molar conductance measurements were made using 10^{-3} M solutions of the complexes in DMF employing a direct reading conductivity meter 303 provided with a cell, of cell constant 1·02. FAB

mass spectra were obtained on a Jeol SX 1021 DA-6000 mass spectrometer using *m*-nitrobenzyl alcohol (NBA) as a matrix.

4. Microbiol screening

4.1 *Bactericidal screening*

Antibacterial activities of the ligand and the soluble complexes were evaluated by the disc diffusion technique [13]. Filter paper (Whatman No. 4) discs (6 mm diameter) were soaked in a solution of the test compounds of 0·5 mg cm^{-3} concentration in DMF and placed on nutrient agar-plates after drying to remove the solvent. The inhibition zones were measured after 24 h. DMF was used as control and gentamicin as the standard drug.

4.2 *Fungicidal screening*

Antifungal activities of the ligand and the soluble complexes were evaluated by the spore germination technique [14]. Solutions of the test compounds were prepared in DMF (0·5 mg cm^{-3}) and placed on the fungus slide. The slides were incubated for 24–72 h at 37°C. A contaminant in the solution indicates 100% growth of fungus which is represented as +, 50% growth by + +, less than 50% growth by + + +, and excellent inhibition by + + + + (see table 7 below in §6.8).

5. Antitumour screening

5.1 *In vitro DNA synthesis inhibition assay*

Jurket and Daltons lymphoma cell suspensions were prepared in a complete medium (RPMI 1640 medium supplemented with penicillin, streptomycin and 10% heat-inactivated foetal calf serum) at concentrations of 10^6 cells cm^{-3} following the literature method [15]. 2×10^5 cells $well^{-1}$ was added to duplicate wells of a 96-well culture plate (Nunc, Denmark). The cells were treated with test compounds at 10 µg cm^{-3} dose and incubated for 24 h at 37°C in a CO_2 incubator. In control sets no treatment was given. After 24 h of incubation, the cells were washed thrice with RPMI 1640 culture medium (without serum) by centrifugation (400 g for 10 min). The cell pellets were resuspended in 0·2 cm^{-3} complete medium containing 1 µci cm^{-3} ^{3}H-thymidine and pulse-labelled for 4 h. The cells were then washed thrice with phosphate buffer saline (PBS), lysed with 1% sodium dodecyl sulphate (SDS) and the lysate was subjected to radioactivity count in a LKB-*b*/-liquid scintillation counter. The percentage inhibition of incorporation was calculated as follows.

$$\% \text{ inhibition} = 1 - (\text{CPM in treated tumour cells}/\text{CPM in untreated tumour cells}) \times 100,$$

where CPM = counts per minute.

5.2 *In vitro growth inhibitory assay*

An MTT assay was used to measure the cytotoxic effect of the ligand and its complexes. The pale-yellow tetrazolium salt, [3-(4,5-dimethylthiazol)-2-yl]-2,5-

diphenyl-2H-tetrazolium bromide] (MTT), was cleaved by active mitochondria to form a dark blue formazan product that can be completely solubilized in acidfied isopropanol and detected by a microtitre plate reader [16]. The assay provides a simple way to detect living and growing cells without using radioactivity. Briefly, 5×10^4 tumour cells (Jurket and Dalton lymphoma) were plated in triplicate in 96-well flat bottom tissue culture plates, and treated with different concentrations of drugs for the time indicated. MTT (0·005 g cm^{-3} in PBS) was added to the cell culture and incubated for 4 h at 37°C in a 5%-CO_2 humidified incubator. The formazan crystals formed during the reaction of active mitochondria with MTT were dissolved in 0·04 N HCl (100 cm^3) in isopropanol and readings were taken in a microtitre plate reader using a 570 nm filter. The average drug concentration (μg cm^{-3}) for 50% inhibition (ID_{50}) of tumour cell-growth was determined by plotting the log of drug concentration vs. the growth rate of tumour cells in the presence of solvent (% control).

5.3 *Morphological evaluation of apoptotic cells*

A drop of cell suspension was air dried, fixed in MeOH and stained with Wright's solution (Accustain Wright stain (modified), Sigma), mounted in a permanent medium and analysed under a light microscope (Leitz Wetzlar, Germany) at 100 × magnification. Apoptotic cells were identified on the basis of morphological features that included contracted cell bodies, condensed, uniformly circumscribed and densely stained chromatin or membrane-bound apoptotic bodies containing one or more nuclear fragments [17]. The percent of apoptotic cells was determined by counting more than 300 cells for at least three different determinations.

5.4 *Percent DNA fragmentation assay*

Quantitative determination of DNA fragmentation was carried out following Sellins and Cohen [18] with slight modifications. Thymocytes (1×10^6 cells cm^{-3}) were lysed in 0·5 cm^3 of *tris*-EDTA buffer, *p*H 7·4, containing 0·2% (*v*/*v*) Triton X-100 and the fragmented DNA was separated from intact chromatin in a microfuge tube (labelled as B) by centrifugation at 13,000 g at 4°C for 10 min. Supernatant containing the fragmented DNA was transferred to another microfuge tube (labelled as T). A volume of 0·5 cm^3 of 25% Cl_3CCO_2H (TCA) was added to each T and B tube and vortexed vigorously. DNA was precipitated overnight at 4°C and collected by centrifugation at 13,000 g and then 80 μl of 5% TCA was added to each pellet. DNA was hydrolyzed by heating at 90°C for 15 min. At this stage a blank was included containing 80 μl of 5% TCA. Finally, 160 μl of freshly prepared DPA reagent (150 mg diphenylamine in 10 cm^3 glacial AcOH, 150 μl conc. H_2SO_4 and 50 μl of MeCHO solution) was added and the tubes were allowed to stand overnight at room temperature to develop colour. 100 μl of this coloured solution was transferred to the wells of a 96-well flat-bottomed Elisa plate and the optical density measured at 600 nm in a microtitre plate reader. The percent DNA fragmentation was calculated as,

$$\text{percent DNA fragmentation} = [T/(T + B)] \times 100,$$

where, T = absorbance of fragmented DNA, $T + B$ = absorbance of total DNA.

6. Results and discussion

All the solid complexes are stable in air. The metal thiocyanate complexes are soluble in DMF and DMSO, but insoluble in other organic solvents, while the metal chloride complexes are also soluble in ethanol, methanol and acetone. The molar conductivity of [Ni(DBtsc-H)(SCN)(H_2O] in 10^{-3} M DMF was found to be 73·4 Ω^{-1} cm^2 mol^{-1} which falls in the range reported for an 1:1 electrolyte [19], indicating solvolysis in DMF, while other complexes show molar conductivities of 33·3–63·4 Ω^{-1} cm^2 mol^{-1}, suggesting their non-electrolytic nature [19]. The following equations represent the formation of the ligand and the complexes.

$$PhCONCS + PhCONHNH_2 \rightarrow PhCONHCSNHNHCOPh,$$
(DBtsc)

$$Mn(SCN)_2 + DBtsc \xrightarrow[\text{Stir}]{\text{EtOH}} [Mn(DBtsc\text{-}H)(SCN] + HSCN,$$

$$M(SCN)_2 + DBtsc \xrightarrow[\text{Reflux}]{\text{EtOH}} [M(DBtsc\text{-}H)(SCN)] + HSCN,$$
(M = Co(II) or Zn(II))

$$Ni(SCN)_2 + DBtsc \xrightarrow[\text{Reflux}]{\text{EtOH}} [Ni(DBtsc\text{-}H)(SCN)(H_2O)] + HSCN,$$

$$Cu(SCN)_2 + DBtsc \xrightarrow[\text{Stir}]{\text{DMF}} [Cu(DBtsc\text{-}H)(SCN)(H_2O)] + HSCN,$$

$$MnCl_2.4H_2O + DBtsc \xrightarrow[\text{Reflux}]{\text{EtOH}} [M(DBtsc)Cl_2] + 4H_2O,$$

$$NiCl_2.6H_2O + DBtsc \xrightarrow[\text{Reflux}]{\text{EtOH}} [Ni(DBtsc\text{-}H)Cl] + HCl + 6H_2O,$$

$$CoCl_2.6H_2O + DBtsc \xrightarrow[\text{Stir}]{\text{EtOH}} [Co(DBtsc\text{-}H)Cl] + HCl + 6H_2O,$$

$$CuCl_2.2H_2O + DBtsc \xrightarrow[\text{Reflux}]{\text{EtOH}} [Cu(DBtsc\text{-}H)Cl] + HCl + 2H_2O,$$

$$ZnCl_2 + DBtsc \xrightarrow[\text{Reflux}]{\text{EtOH}} [Zn(DBtsc\text{-}H)] + HCl.$$

6.1 *Magnetic moments*

The magnetic moment value (5·8 BM) for [Mn(DBtsc-H)(SCN)] and [Mn(DBtsc)Cl_2], indicates the presence of five unpaired electrons. [Co(DBtsc-H)(SCN)] and [Co(DBtsc-H)Cl] exhibit m_{eff} = 4·7–4·8 BM (table 1). [Ni(DBtsc-H)(SCN)(H_2O)] and [Ni(DBtsc-H)Cl] show magnetic moments of 3·3 and 3·2 BM respectively, indicating their tetrahedral geometry. Magnetic moments of [Cu(DBtsc-H)(SCN)(H_2O)] and [Cu(DBtsc-H)Cl] are 1·9 and 1·8 BM respectively, as expected for the presence of one unpaired electron.

Table 1. Analytical data and physical properties of the 1,4-dibenzoyl-3-thiosemicarbazide complexes.

	Colour	Yield (%)	Found (calcd.) (%)						m.p. (°C)	μ_{eff} (BM)	Molar conductivity (Ω^{-1} cm^2 mol^{-1})
			M	S	C	H	N	SCN/Cl			
	White	70	–	9·6 (10·6)	60·2 (60·1)	4·5 (4·3)	13·8 (14·0)	–	172	–	–
-H)(SCN)]	Light yellow	60	12·4 (13·4)	15·3 (15·5)	46·5 (46·6)	2·8 (2·9)	13·5 (13·6)	13·9 (14·1)	>300	5·8	63·4
$_2$]	Yellowish	65	12·5 (12·9)	7·4 (7·5)	41·9 (42·3)	2·9 (3·0)	9·7 (9·8)	16·8 (16·7)	>300	5·8	52·3
-H)(SCN)]	Dirty green	70	13·9 (14.2)	15·4 (15·4)	45·8 (46·2)	2·7 (2·8)	12·9 (12·4)	13·8 (13·9)	>300	4·7	57·1
-H)Cl]	Dirty green	70	14·4 (14·9)	7·9 (8·1)	45·4 (45·7)	2·8 (3·0)	10·5 (10·6)	8·9 (9·0)	255	4·8	61·7
-H)(SCN)(H_2O)]	Dirty yellow	65	14·2 (13·5)	14·7 (14·8)	44·4 (44·3)	3·1 (3·2)	12·7 (12·9)	12·6 (13·4)	>300	3·1	73·4
-H)Cl]	Gray	60	14·7 (14·9)	7·7 (8·1)	45·5 (45·8)	2·9 (3·0)	10·6 (10·7)	8·6 (9·0)	>300	3·0	56·8
-H)(SCN)(H_2O)]	Black	65	14·3 (14·5)	14·5 (14·6)	43·7 (43·8)	2·9 (3·1)	12·6 (12·7)	12·9 (13·2)	233	1·9	42·8
-H)Cl]	Black	65	15·8 (15·9)	7·9 (8·0)	45·2 (45·3)	2·8 (3·0)	10·4 (10·5)	8·9 (8·9)	>300	1·8	39·2
-H)(SCN)]	Dirty white	60	15·2 (15·5)	15·3 (15·2)	45·4 (45·5)	2·7 (2·8)	9·8 (9·9)	13·6 (13·7)	279	dia*	35·7
-H)Cl]	Off white	55	16·2 (16·3)	7·8 (8·0)	44·9 (45·1)	2·8 (3·0)	10·4 (10·5)	8·7 (8·8)	269	dia	33·3

= diamagnetic

6.2 *Electronic spectra*

In the absence of a *d–d* band, the value of magnetic moment (5·8 BM) and infrared spectral data suggest tetrahedral arrangement of the ligands around manganese (II). [Co(DBtsc-H)(SCN)] shows four bands at 15435, 16615, 17185 and 19015 cm^{-1} (table 2), while [Co(DBtsc-H)Cl] exhibits a band at 17360 cm^{-1} assigned to the $^4A_2 \rightarrow {}^4T_1$ (*F*) (ν_3) transition for tetrahedral geometry of [Co(DBtsc-H)X] [X = SCN or Cl]. Nickel (II) complexes exhibit two bands at 16025–16665 and 20205–21185 cm^{-1}, assigned to the $^3T_1$ (*F*) $\rightarrow {}^3T_1$ (*P*) and charge transfer (*ct*) transitions respectively in tetrahedral geometry [20]. [Cu(DBtsc-H)Cl] shows a band at 16130 cm^{-1} assigned to the envelope of $^2B_{1g} \rightarrow {}^2A_{1g}$, $^2B_{2g}$ and ^2E_g transitions, while [Cu(DBtsc-H)(SCN)(H_2O)] shows two bands at 16995 and 20835 cm^{-1} due to the envelope of $^2B_{1g} \rightarrow {}^2A_{1g}$, $^2B_{2g}$ and ^2E_g transitions, and *ct*, suggesting a square-planar structure for the copper (II) complexes [20].

6.3 *IR spectra*

The IR spectrum of the ligand (table 3) in KBr shows bands at 3059, 3142 and 3271 cm^{-1} due to the presence of three NH groups which are also present in [Mn(DBtsc)Cl_2]. The band at 3271 cm^{-1} is absent in other metal (II) thiocyanato and chloro complexes (table 3), indicating loss of a proton via enolisation/thioenolisation in the deprotonated complexes. The peaks at 1633 and 1666 cm^{-1} are assigned to the C=O groups attached to the benzene rings A and B, respectively. The ν(C=O) band of the ligand at 1666 cm^{-1} shows a negative shift of 10–42 cm^{-1} in [M(DBtsc-H)(SCN)] [M = manganese (II), cobalt (II) or zinc (II)] and [M(DBtsc-H)Cl] [M = cobalt (II), nickel (II), copper (II) or zinc (II)], indicating bonding through the amide oxygen attached to the benzene ring B. The ν(C=O) band of the ligand at 1633 cm^{-1} is absent in these complexes, but the presence of a new band at 1590–1605 cm^{-1}, due to the ν(N=C) of NCO, indicates removal of a hydrazinic proton via enolisation, and subsequent participation of the enolic oxygen in bonding. The spectrum of [Mn(DBtsc)Cl_2], however, shows a negative shift of 10 cm^{-1} in ν(C=O) of the hydrazide part of the ligand, showing bonding through the carbonyl oxygen. The ν(N–N) ligand band at 999 cm^{-1} shows a positive shift of 33–83 cm^{-1} in the complexes, due to bonding through one hydrazinic nitrogen [7]. Thioamide bands I[δ(NH) + ν(CN)], III[(ν(CN) + δ(NH)] and IV[ν(C=S)] observed at 1579, 1275 and 877 cm^{-1} respectively in the ligand do not undergo considerable change in the complexes, ruling out the possibility of bonding through the >C=S group. In the thiocyanate complexes, ν(C≡N) is observed in

Table 2. UV-Visible spectral data of the complexes and their assignments.

Complex	Band max (cm^{-1})	Assignments
[Co(DBtsc-H)(SCN)]	15435, 16615, 17185, 19015*	$^4A_2 \rightarrow {}^4T_1(F)n_3$
[Co(DBtsc-H)Cl]	17360	
[Ni(DBtsc-H)(SCN)(H_2O)]	16665, 20205*	$^3T_1(F) \rightarrow {}^3T_1(P)$
[Ni(DBtsc-H)Cl]	16025, 21185*	
[Cu(DBtsc-H)(SCN)(H_2O)]	16995, 20835*	Envelope of $^2B_{1g} \rightarrow {}^2A_{1g}$, $^2B_{2g}$ and ^2E_g,
[Cu(DBtsc-H)Cl]	16130	Envelope of $^2B_{1g} \rightarrow {}^2A_{1g}$, $^2B_{2g}$ and ^2E_g

*charge transfer

Table 3. Important IR spectral bands (cm^{-1}) and their assignment.

	n(NH)	*n*(C=O)/*n*(NCO)	Thioamide I [*b*(NH) + *n*(CN)]	Thioamide III [*n*(CN) + *b*(NH)]	Thioamide IV *n*(C=S)	*n*(N–N)	*n*(SCN)
	3059, 3142, 3271	1666, 1633	1579	1275	877	999	–
-H)(SCN)]	3090, 3213, –	1643, 1597	1575	1271	878	1074	2083
$_2$]	3190, 3271, 3395	1665, 1623	1575	1275	880	1082	–
-H)(SCN)]	3080, 3213, –	1639, 1590	1577	1273	880	1070	2095
-H)Cl]	3070, 3171, –	1631, 1602	1575	1280	875	1070	–
-H)(SCN)(H_2O)]	3110, 3125, –	1668, 1590	1577	1271	877	1070	2119
-H)Cl]	3075, 3221, –	1641, 1590	1579	1281	877	1032	–
-H)(SCN)(H_2O)]	3057, 3202, –	1668, 1604	1574	1275	878	1068	2091
-H)Cl]	3090, 3224, –	1624, 1590	1575	1282	877	1074	–
-H)(SCN)]	3060, 3225, –	1656, 1605	1575	1273	877	1082	2081
-H)Cl]	3060, 3234, –	1656, 1603	1575	1275	880	1070	–

the region of 2081–2119 cm^{-1}, suggesting bonding through the nitrogen of the thiocyanato group [21]. IR spectral data show that the ligand acts as a neutral bidentate in $[Mn(DBtsc)Cl_2]$, mononegative bidentate in $[M(DBtsc\text{-}H)(SCN)(H_2O)]$ [M = nickel (II) or copper (II)], bonding through the carbonyl/enolic oxygen and the hydrazinic nitrogen. It, however, behaves as a mononegative tridentate in [M(DBtsc-H)(SCN)] [M = manganese (II), cobalt (II) or zinc (II)] and [M(DBtsc-H)Cl] [M = cobalt (II), nickel (II), copper (II) or zinc (II)], the bonding sites being the carbonyl as well as enolic oxygens and N^2-nitrogen of the ligand (figure 2).

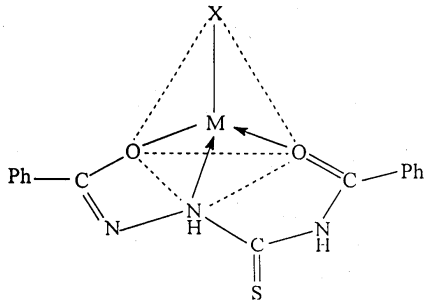

[M(DBtsc-H)X] [M = Mn, Co or Zn], [X = SCN]
[M(DBtsc-H)X] [M = Co, Ni or Zn], [X = Cl]

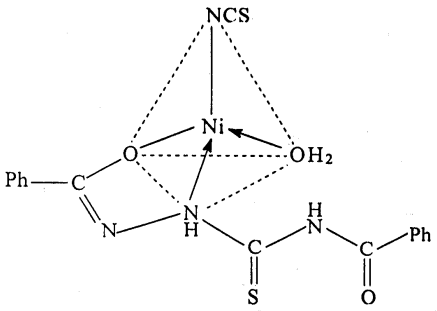

[Ni(DBtsc-H)(SCN)(H_2O)]

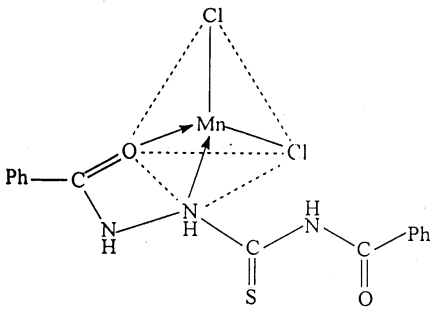

[Mn(DBtsc)Cl_2]

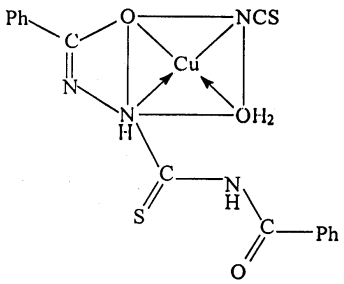

[Cu(DBtsc-H)(SCN)(H_2O)]

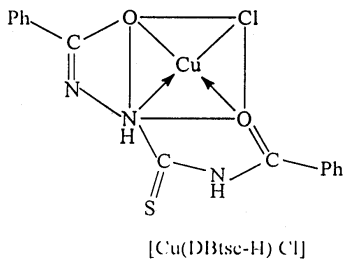

[Cu(DBtsc-H)Cl]

Figure 2. Proposed structure of the complexes.

6.4 *NMR spectra*

The ^{1}H-NMR spectrum of the ligand (DBtsc) shows three signals at *d* 10·83 (*s*, 1H), 11·46 (*s*, 1H) and 12·13 (*s*, 1H) ppm due to the presence of three NH groups. Signals at *d* 7·73–8·13 (*m*, 10H) ppm are assigned to the ring protons (table 4). The ^{13}C-NMR spectrum of DBtsc (table 5) shows eleven signals due to the presence of fifteen carbon atoms. Two signals at *d* 167·89 and 164·64 ppm are due to the presence of carbonyl groups attached to the benzene rings A and B respectively. The signal at *d* 180·62 ppm is assigned to the C=S carbons. The chemical shift for the ring carbons are (*d*, ppm) C(1), 133·22; C(2,6), 127·53; C(3,5), 128·56; C(4), 131·92; C′(1), 132·62; C′(2,6), 128·77; C′(3,5), 127·75; C′(4), 132·13. ^{1}H-NMR spectra of [Zn(DBtsc-H)(SCN)] and [Zn(DBtsc-H)Cl] show two signals at *d* 10·53–10·58 (*s*, 1H) and 11·40–11·42 (*s*, 1H) ppm, indicating the presence of two-NH protons and loss of N^{1}H proton via enolisation. Signals at 7·60 to 7·90 (*m*, 10H) ppm are assigned to the ring protons. ^{13}C-NMR spectra exhibit signals at 180·61 and 180·65 ppm for the C=S carbon, which remain practically unchanged, indicating non-participation of the thione sulphur in bonding. The carbonyl signals show an upfield shift of 0·13–0·15 ppm in [Zn(DBtsc-H)(SCN)] and [Zn(DBtsc-H)Cl], indicating bonding through the enolic as well as carbonyl oxygen atoms.

6.5 *ESR spectra*

The ESR spectrum of [Cu(DBtsc-H)(SCN)(H_2O] at room temperature shows two signals with $g_{\|} = 2{\cdot}08$ and $g_{\perp} = 2{\cdot}05$. [Mn(DBtsc-H)(SCN)] shows one signal, $g_{av} = 2{\cdot}01$. These ESR features indicate square-planar and tetrahedral geometries for the copper (II) and manganese (II) complexes respectively.

Table 4. ^{1}H-NMR data of DBtsc and the complexes (*d*, ppm).

Compound	NH	NH_2	Benzene ring
BAH[a]	9·86 (*br*, H)	3·86 (*s*, 2H)	7·86 (*t*, 2H), 7·46 (*d*, 3H)
DBtsc	12·13 (*s*, 1H), 11·46 (*s*, 1H), 10·83 (*s*, 1H)	–	7·73–8·13 (*m*, 10H)
[Zn(DBtsc-H)(SCN)]	11·40 (*s*, 1H), 10·58 (*s*, 1H)	–	7·60–7·90 (*m*, 10H)
[Zn(DBtsc-H)Cl]	11·42 (*s*, 1H), 10·53 (*s*, 1H)	–	7·66–7·93 (*m*, 10H)

[a]Benzoic acid hydrazide

Table 5. ^{13}C-NMR spectra data (*d*, ppm).

Compound	>C=O	>C=S	C(1)	C(2, 6)	C(3, 5)	C(4)	C′(1)	C′(2, 6)	C′(3, 5)	C′(4)
Benzamide	168·27	–	–	–	–	–	131·32	128·23	127·58	134·30
BAH[a]	166·37	–	133·38	127·15	128·56	131·37	–	–	–	–
DBtsc	167·89, 164·64	180·62	133·22	127·53	128·56	131·92	132·62	128·77	127·75	132·13
[Zn(SBtsc-H)(SCN)]	167·76, 164·49	180·61	134·79	127·42	128·56	129·37	133·27	128·77	127·69	132·08
[Zn(SBtsc-H)Cl]	167·75, 164·49	180·65	134·79	127·47	128·56	129·36	133·27	12·72	127·65	132·08

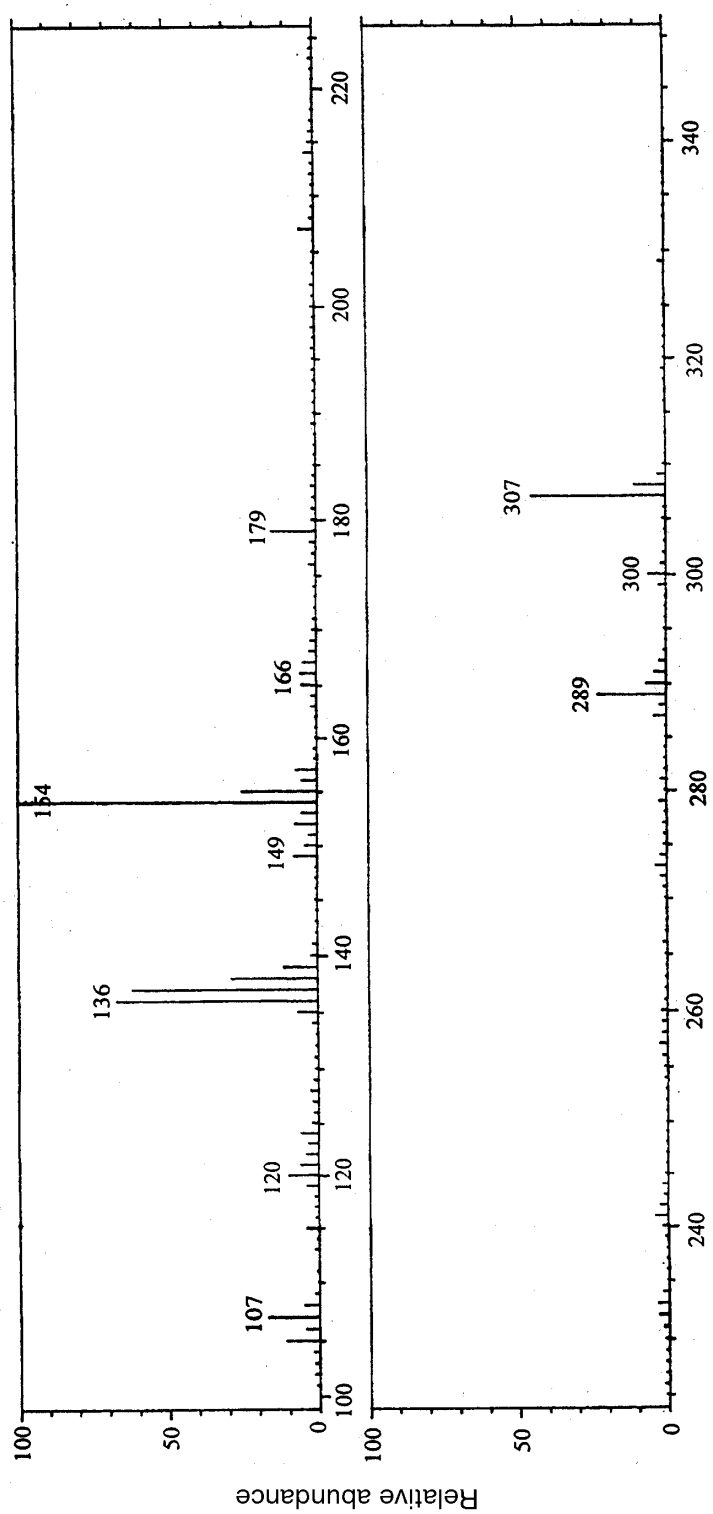

FAB mass spectrum of DBtsc.

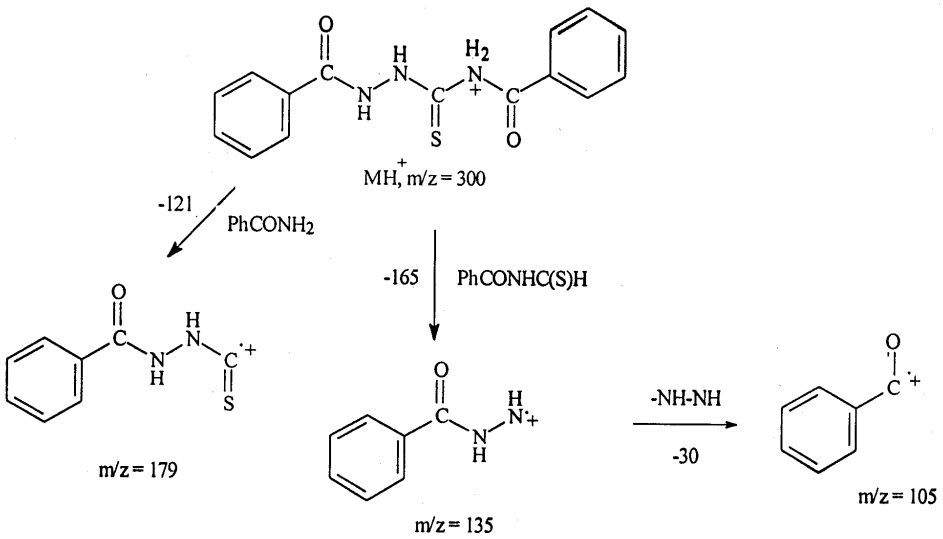

Figure 3b. Fragmentation scheme for DBtsc.

6.6 *FAB mass spectra*

The molecular ion peak MH^+ for DBtsc is observed at $m/z = 300$. Other important peaks at 179 and 165 correspond to the release of $PhCONH_2$ and PhCONHNH from the MH^+. The molecular ion peak for [Ni(DBtsc-H) (SCN)(H_2O)] is observed at $m/z = 433$. The other important peaks at 415, 310, 233 and 175 correspond to the release of H_2O, PhCO, Ph and SCN respectively, from the fragments of [Ni(DBtsc-H)(SCN)(H_2O)]. Other peaks in the FAB mass spectrum account for the release of SCN, Ph and PhCO from the anhydrous complex and its successive fragments. FAB mass spectra of the ligand (DBtsc) and [Ni(DBtsc-H)(SCN)(H_2O)] are depicted in figures 3a and 4a, while the fragmentation schemes are shown in figures 3b and 4b.

6.7 *Bactericidal screening*

Results of antibacterial screening, shown in table 6, indicate that all thicyanato and chloro complexes, inhibit the growth of *Pseudomonas flauracences*, whereas, the ligand and other complexes are inactive against other seven tested bacteria.

6.8 *Fungicidal screening*

Results of antifungal activity are shown in table 7. The ligand, [M(DBtsc-H)Cl] [M = cobalt (II) or nickel (II)] and [Zn(DBtsc-H)(SCN)] show moderate activity against *Aspergillus flavus*, while [M(DBtsc-H)(SCN)] [M = manganese (II) or cobalt (II)], [Ni(DBtsc-H)(SCN)(H_2O)], [Mn(DBtsc)Cl_2] and [Zn(DBtsc-H)Cl] show good antifungal activity against *A. flavus*. The ligand shows poor activity, while [M(DBtsc-H)(SCN)] [M = cobalt (II) or zinc (II) and [Zn(DBtsc-H)Cl] show moderate activity against *Aspergillus niger*, [Mn(DBtsc-H)(SCN)], [Ni(DBtsc-H)(SCN)(H_2O)], [M(DBtsc-H)Cl] [M = cobalt (II) or nickel (II)] and [Mn(DBtsc)Cl_2] show good

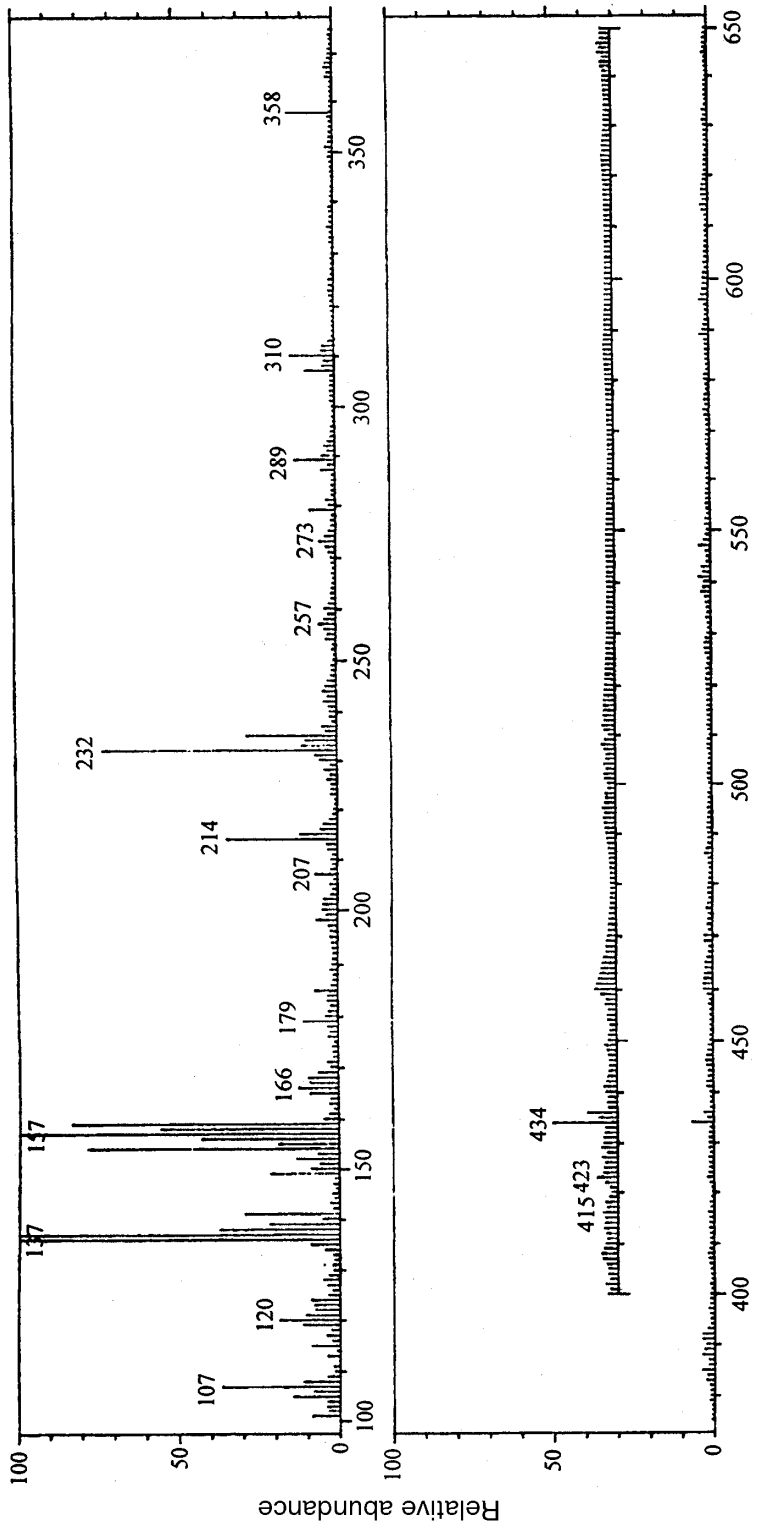

FAB mass spectrum of [Ni(DBtsc -H)(SCN)(H_2O)].

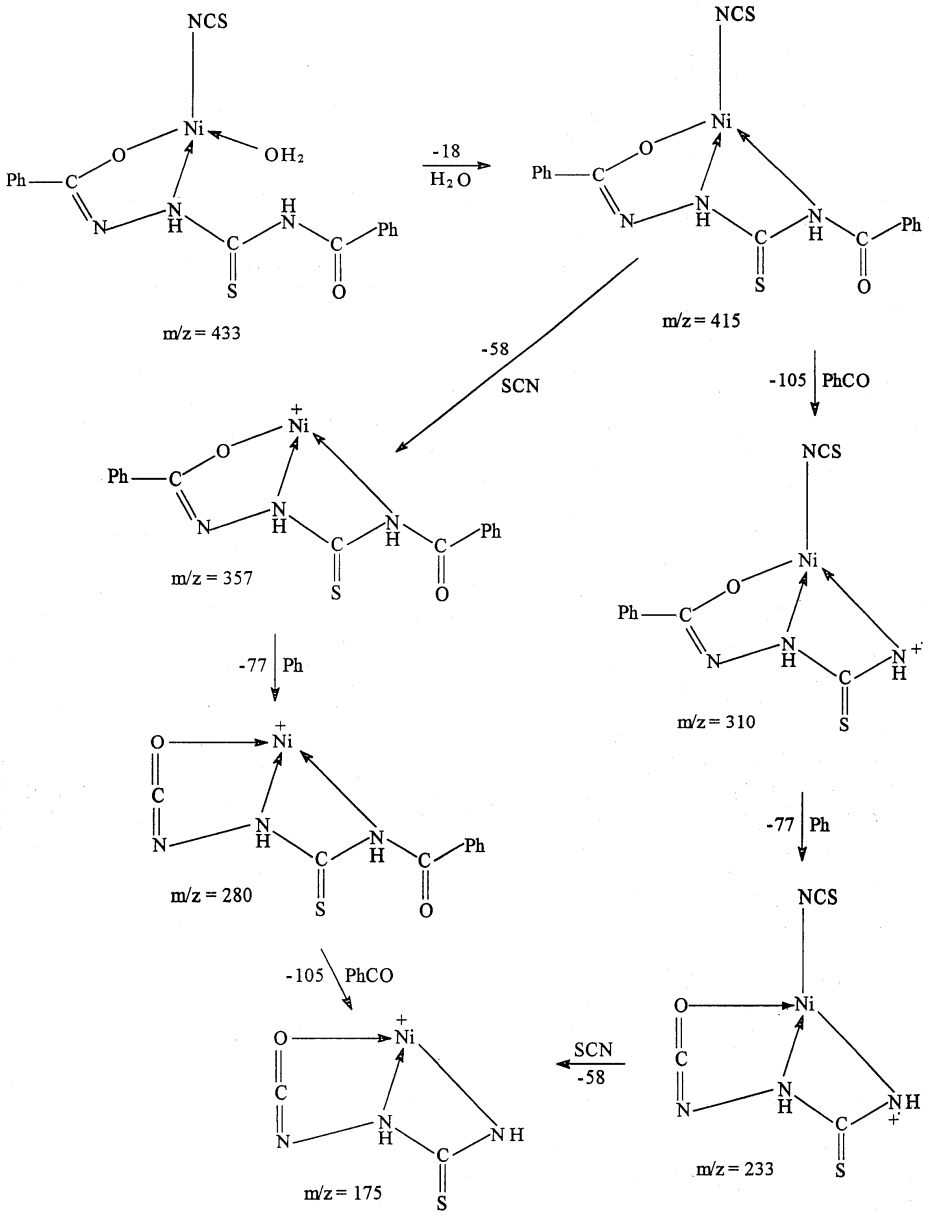

Figure 4b. Fragmentation scheme for [Ni(DBtsc-H)(SCN)(H_2O)].

antifungal activity against *A. niger*. [Cu(DBtsc-H)(SCN).H_2O] and [Cu(DBtsc-H)Cl] exhibit excellent antifungal activity against both the fungi.

6.9 *Antitumour screening*

Results of antitumour screening indicate that the percentage of cell growth in the presence of DBtsc is less than its Cu(II) thiocyanato/chloro complexes. Percentage

inhibition of thymidine incorporation data (table 8) show that the ligand has a pronounced inhibitory effect on DNA synthesis, whereas its metal complexes have less inhibitory effect. The ligand showed higher inhibition of thymidine incorporation in Jurket and Daltons lymphoma tumour cells than [Cu(DBtsc-H)(SCN)(H_2O)] and [Cu(DBtsc-H)Cl]. Further, the MTT assay performed at 10 μg cm^{-3} corroborated the same finding as is evident from the low ID_{50} values (table 9) for the ligand than those of [Cu(DBtsc-H)(SCN)(H_2O)] and [Cu(DBtsc-H)Cl]. To understand the probable mechanism of the antitumour action of these compounds, the mode of cell death was studied and found to be due to apoptosis. The percentages of these apoptotic cells were higher for the ligand than for the complexes. Percentage DNA fragmentation data (table 9) further support the above findings by showing higher values for the ligand

Table 6. Antibacterial activity of DBtsc and its complexes.

	Bacteria							
Compound	a	b	c	d	e	f	g	h
DBtsc	–	–	–	–	–	–	–	–
[Mn(DBtsc-H)(SCN)]	–	–	–	–	+	–	–	–
[Mn(DBtsc)Cl_2]	–	–	–	–	+	–	–	–
[Co(DBtsc-H)(SCN)]	–	–	–	–	+	–	–	–
[Co(DBtsc-H)Cl]	–	–	–	–	+	–	–	–
[Ni(DBtsc-H)(SCN)(H_2O)]	–	–	–	–	+	–	–	–
[Ni(DBtsc-H)Cl]	–	–	–	–	+	–	–	–
[Cu(DBtsc-H)(SCN)(H_2O)]	–	–	–	–	+	–	–	–
[Cu(DBtsc-H)Cl]	–	–	–	–	+	–	–	–
[Zn(DBtsc-H)(SCN)]	–	–	–	–	+	–	–	–
[Zn(DBtsc-H)Cl]	–	–	–	–	+	–	–	–
Gentamicin	–	–	–	–	+	–	–	–

a = *Siglabeoyddi*, b = *Citroductree freendii*, c = *E. coli*, d = *Pseudomonas aeruginosa*, e = *Pseudomonas flauracences*, f = Step 25923, g = *P. vulgaris*, h = *B. subtilis*

Table 7. Antifungal activity of DBtsc and its complexes.

	Inhibition of spore germination (%)	
Compound	*A. flavus*	*A. niger*
DBtsc	+ +	+
[Mn(DBtsc-H)(SCN)]	+ + +	+ + +
[Mn(DBtsc)Cl_2]	+ + +	+ + +
[Co(DBtsc-H)(SCN)]	+ + +	+ +
[Co(DBtsc-H)Cl]	+ +	+ + +
[Ni(DBtsc-H)(SCN)(H_2O)]	+ + +	+ + +
[Ni(DBtsc-H)Cl]	+ +	+ + +
[Cu(DBtsc-H)(SCN)(H_2O)]	+ + + +	+ + + +
[Cu(DBtsc-H)Cl]	+ + + +	+ + + +
[Zn(DBtsc-H)(SCN)]	+ +	+ +
[Zn(DBtsc-H)Cl]	+ + +	+ +

Table 8. Cell proliferation assay and percentage inhibition of thymidine incorporation.

Compound	Cell growth (%)	Thymidine incorporation (%)	
		Jurket	DL*
Tumour cell	100	–	–
DBtsc	24·90	74·75	73·28
[Cu(DBtsc-H)(SCN)(H_2O)]	51·32	47·19	48·72
[Cu(DBtsc-H)Cl]	52·69	45·68	47·84

*Dalton's lymphoma

Table 9. *In vitro* ID_{50}, percentage apoptosis and percentage DNA fragmentation for DBtsc and its metal complexes.

Compound	ID_{50} values		% Apoptosis		% DNA fragmentation	
	Jurket	DL*	Jurket	DL	Jurket	DL
Tumour cell	–	–	36·52	35·35	39·21	40·43
DBtsc	1·2	1·3	88·62	86·42	90·20	84·73
[Cu(DBtsc-H)(SCN)(H_2O)]	3·7	3·2	41·21	43·92	43·92	47·53
[Cu(DBtsc-H)Cl]	3·8	3·7	40·10	42·62	41·23	43·82

ID_{50} = inhibitory dose (μg cm^{-3}) for 50% tumour regression; *DL = Dalton's lymphoma

than for [Cu(DBtsc-H)(SCN)(H_2O)] and [Cu(DBtsc-H)Cl]. Therefore, the ligand possesses higher antitumour activity as compared to its metal complexes. The above finding is in accord with the *in vivo* antitumour activity of N-salicyloyl-N′-(2-furanthiocarbonyl) hydrazine which is reported to be better than its copper (II) complexes [22]. Results show that the growth inhibition of tumour cells is due to apoptosis in the case of the ligand, whereas the antitumour activity of the copper (II) complexes is not due to apoptosis. It appears that the metal complexes inhibit cellular growth by binding with DNA [22].

7. Conclusions

The ligand DBtsc has been found to bind as neutral bidentate in [Mn(DBtsc)Cl_2], as mono negative bidentate in [M(DBtsc-H)(SCN)(H_2O)] [M = nickel (II) or copper (II)], and as mononegative tridentate in [M(DBtsc-H)(SCN)] [M = manganese (II), cobalt (II) or zinc (II)] and [M(DBtsc-H)Cl] [M = cobalt (II), nickel (II), copper (II) or zinc (II)]. The ligand exhibits better antitumour activity than Cu (II) thiocynato/chloro complexes against Jurket and Daltons lymphoma cell lines.

Acknowledgements

We thank Dr G Nath, Institute of Medical Sciences, BHU for bactericidal screening. Thanks are also due to Dr N K Dubey and Mr Rajesh Kumar Dubey, Department of Botany, BHU for fungicidal screening.

References

1. Buu-Hoi N P, Loc T B and Xuong N D 1955 *Bull. Soc. Chim. Fr*. 694
2. Ali M A and Livingston S E 1974 *Coord. Chem. Rev.* **13** 101
3. Petering H G, Buskik H H and Underwood G E 1964 *Cancer Res.* **64** 367
4. El-Asmy A A 1989 *Bull. Soc. Chim. Fr.* 171
5. El-Asmy A A 1988 *J. Chin. Chem. Soc.* **35** 29
6. Mostafa M M, Shallaby A M and El-Asmy A A 1981 *Transition Met. Chem.* **6** 303
7. El-Asmy A A, Al-Ansi T Y, Amin R R and Mourin M 1990 *Polyhedron* **9** 2029
8. Aggarwal R C and Yadav R B S 1976 *Transition Met. Chem.* **1** 139; Aggarwal R C and Yadav R B S 1975 *Indian J. Chem.* **A13** 727
9. Amberlang J C and Johnson T S 1939 *J. Am. Chem. Soc.* **61** 632
10. Curtius T 1894 *J. Prakt. Chem*. **52** 278
11. Nakai R, Sugai M and Nakao H 1957 *Phasm. Bull. (Tokyo)* **5** 576
12. Vogel A I 1969 *A text book of quantitative inorganic analysis* 3rd edn (London: ELBS, Longman)
13. Verma R S and Imam S A 1973 *Indian J. Microbiol.* **13** 45
14. Adisa V A 1985 *Indian Phytopath.* **38** 277
15. Sodhi A and Singh S M 1986 *Int. J. Immunopharmacol*. **8** 701
16. Mosamann T R, Cherwinski H, Bond M V, Giedliv M A and Coffmann R 1986 *J. Immunol.* **13** 2348
17. Kerr J F R, Wyllie A H and Currie A R 1972 *Br. J. Cancer* **26** 239
18. Selline K S and Cohen J J 1987 *J. Immunol.* **139** 3199
19. Geary W J 1971 *Coord. Chem. Rev*. **7** 81
20. Lever A B P 1984 *Inorganic electronic spectroscopy* 2nd edn (Amsterdam: Elsevier)
21. Nathan L C 1974 *J. Chem. Educ*. **51** 285
22. Agrawal S, Singh N K, Aggarwal R C, Sodhi A and Tandon P 1986 *J. Med. Chem.* **29** 199